Konovalov, Igor; Emelianov, Vitali

Hot carrier solar cell as thermoelectric device

Original published in:

Energy Science & Engineering, ISSN 2050-0505, ZDB-ID 27203396. - Chichester [u.a.] : Wiley. - 5 (2017), 3, p. 113-122.

Original published: 2017-06-26
ISSN (online): 2050-0505
DOI: 10.1002/ese3.159
URL: https://doi.org/10.1002/ese3.159
[*Visited:* 2018-09-18]

Energy Science & Engineering

Open Access

RESEARCH ARTICLE

Hot carrier solar cell as thermoelectric device

Igor Konovalov[1] & Vitali Emelianov[1,2]

[1]Ernst Abbe University of Applied Science in Jena, Carl Zeiss Promenade 2, 07745 Jena, Germany
[2]Thuringian Postgraduate School of Photovoltaics "Photograd", Institute of Physics, Technical University Ilmenau, 98684 Ilmenau, Germany

Keywords
Double heterostructure, kinetic transport theory, prototype hot carrier solar cell, Seebeck effect

Correspondence
Igor Konovalov, Ernst Abbe University of Applied Science, Carl Zeiss Promenade 2, 07745 Jena, Germany. E-mail: igor.konovalov@fh-jena.de

Funding Information
Carl Zeiss Foundation, Land Thüringen (Grant/Award Number: 'Photograd', 'RFAproPV'), European Commission (Grant/Award Number: 'EFRE RFAproPV').

Received: 21 November 2016; Revised: 28 April 2017; Accepted: 12 May 2017

***Energy Science and Engineering* 2017; 5(3): 113–122**

doi: 10.1002/ese3.159

Abstract

Improvement of solar cell efficiency beyond the Shockley–Queisser limit requires introduction of new physical concepts. One such concept is hot carrier solar cell, proposed more than three decades ago and still not impressively demonstrated in experiment. Here we show that hot carrier solar cell may be considered as thermoelectric device based on Seebeck effect. This enables one to describe the operation of hot carrier solar cell in a simple way. We fabricated a prototype of the hot carrier solar cell showing open circuit voltage at room temperature larger than the band gap in the absorber material. Extrapolation of open circuit voltage to absolute zero temperature results in barrier height depending on light intensity, interpreted by splitting of quasi-Fermi levels between the regions of different carrier temperature. Properties of the prototype solar cell may be described by kinetic transport theory as well as from the point of view of the thermoelectric theory.

Introduction

The idea of hot carrier solar cell was proposed by Ross and Nozik in attempt to overcome Shockley-Queisser efficiency limit of 31% at 1 Sun (or 41% at full concentration) in a simple photovoltaic device [1]. Conceptual implementations of Würfel and other researchers are known [2, 3] and are presented in the following in some detail. Figure 1 shows the classical hot carrier cell concept consisting of light absorber with hot electron gas and two semiconductors with energy selective contacts (ESC) at the interfaces. The ESC filter out carriers having certain energies. The carrier cooling is suppressed, but Auger and radiative recombination mechanisms are considered. The doping concentration in the outer semiconductors can be chosen such that the carrier density in the bands at the energies of selective contacts is sufficient to maintain the same flux in both directions through the energy selective contacts. At this condition, there is no energy flow through the energy selective contacts, so that the electron gas in the absorber is only heated by the Sun but can be cooled only by photonic reemission. The heating will stop at the thermodynamic equilibrium with the Sun, when the radiative recombination reverts the radiation to the Sun (through the concentrator optics not shown in the Figure) in each arbitrary spectral region in accordance with detailed balance principle. The Auger recombination does not change the energy of the gas in the absorber, because all the particles involved remain in the absorber. Similarly, the outer semiconductors maintain the same temperature as the ambient. In the Carnot process, the gas is at thermodynamic equilibrium in turn with the heater and with the cooler during the isothermal processes. Similarly, the process in Figure 1 is reversible process and has the Carnot efficiency. Therefore, Figure 1 represents a perfect solar cell with the thermodynamic efficiency never to be topped because the Carnot efficiency cannot be exceeded. The photovoltaic efficiency is achieved when a reversible heat engine is optimally driven off equilibrium, resulting in the photovoltaic efficiency limit

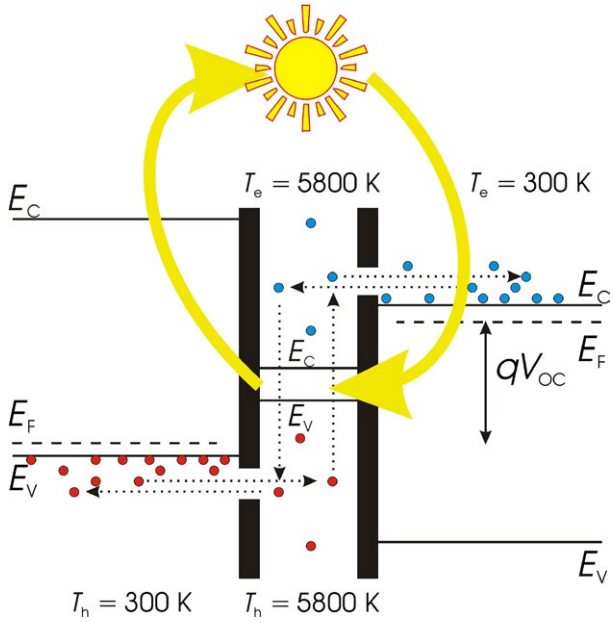

Figure 1. Hot carrier solar cell structure at simultaneous equilibrium with the heater (Sun) and the cooler (ambient) at open circuit condition. $T_{e,h}$ is the temperature of the electron and hole gas.

of at least 85% (Fig. 2A, [4]. This fact is the reason for a continued work at hot carrier solar cell concept throughout the last three decades. Unfortunately, no experimental proof of this hot carrier concept operating at room temperature was attained so far. We modified this concept by replacing the ideal energy selective contacts with the energy barriers being the band offsets at the interfaces (Fig. 2B, [5, 6]. The modified process is, however, thermodynamically nonreversible. A narrow band gap absorber harvests solar radiation in a wide spectral range, and the output voltage is larger than the band gap energy of the absorber semiconductor.

The cell operation is usually described from the point of view of the kinetic transport theory by consideration of quasi-equilibrium thermal emission of the hot carriers from the absorber material into the energy filtering structure. This emission may be described in simple cases by the thermionic emission theory [3, 6–10], being a kinetic transport theory. Kinetic theories are in principle well-suited to describe charge transport in the solar cell; however, the description is rather complex in various specific cases.

Seebeck Theory of Hot Carrier Solar Cell

From the point of view of the thermodynamics, a hot carrier solar cell is a typical thermoelectric device. One can imagine a solar cell being a black body absorber

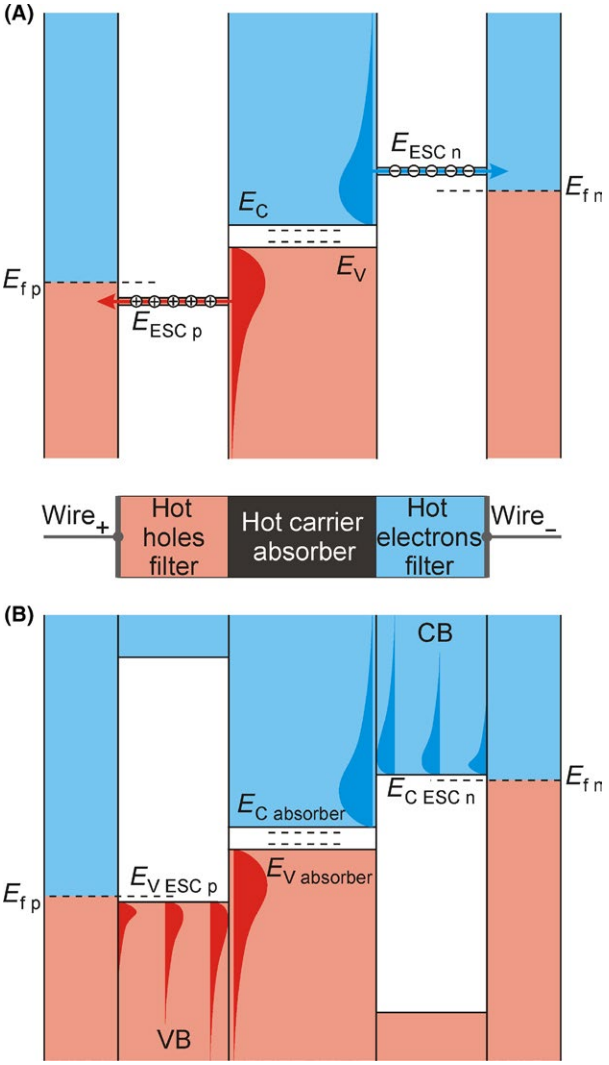

Figure 2. Conceptual implementations of hot carrier solar cells: (A) classical hot carrier cell concept [2]; (B) novel concept [5, 6], discussed here. Energy distribution of hot electrons and holes are shown in the absorber layer: E_V and E_C are energy of the valence and the conduction band edges in the absorber. The energy filters provide energy selective transfer of the hot carriers from the absorber to the metal contacts. VB and CB are the valence and conduction bands in the energy selective layers around the absorber; E_{ESC} are the energy of band edges in the energy selective contacts. Three stages of carrier thermalization in the energy selective contacts are shown: (1) truncated carrier distribution from the absorber being far away from thermal equilibrium; no temperature or Fermi level can be ascribed here; (2) thermalized carrier distribution at a lower temperature than in the absorber; (3) carrier distribution after cooling down to the ambient temperature.

attached to a thermoelectric converter (Fig. 3A). Typical efficiencies of the thermoelectric converters are below 10%, limiting the efficiency of this solar thermal cell. In the solar thermal cell, the lattice of the absorber material is heated by the Sun, and the electron gas of a thermocouple gets heated from the lattice. This circumstance has two

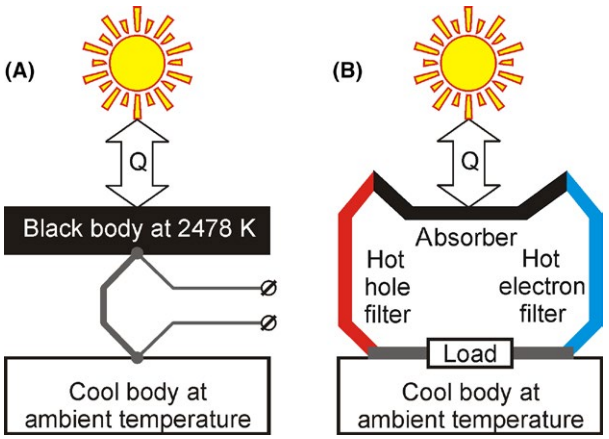

Figure 3. Hot carrier solar cell as thermoelectric device. Model (A) utilizes a conventional thermoelectric converter, attached to a black body absorber. Model (B) is hot carrier solar cell utilizing energy selective filtering of hot carriers from absorber.

drawbacks for efficient energy conversion: (1) in attempt to increase the Carnot efficiency, the temperature of the black body should be high (ideally 2478K, as shown in [11], but most of materials will melt or at least degrade at this high temperature; and (2) Solar heat is partially lost by the lattice thermal conductivity via the phonons. In a hot carrier solar cell both problems may be solved, because the electron gas is heated by the solar radiation directly, rather than via the lattice, which remains cold (Fig. 3B). In both cases the open circuit voltage results from diffusion of the hot carriers in the bulk materials.

Thus, we discuss the hot carrier solar cell as a thermoelectric device, based on Seebeck effect. Being a bulk rather than an interface effect, Seebeck effect determines the open circuit voltage of the hot carrier solar cell independently of the band offsets. Remarkably, Seebeck coefficient shows transitivity, whereas the band offsets do not. The open circuit voltage of a multilayer structure, as it is proposed for the hot carrier solar cells (Fig. 2B), is simply determined by the difference of Seebeck coefficients in the materials where the thermal gradient is large, being typically the energy selective contacts. Seebeck coefficient of the absorber material, staying at constant high electron temperature, makes no influence here. As a result, energy filtering at interfaces between the absorber and the energy selective contacts does not define the open circuit voltage, since it is determined by the bulk Seebeck effect. This finding does not contradict the thermionic theory, because an appropriate band bending may substitute for the band offset during the formation of the energy barrier. Although a specific narrow band energy selective contact material may show large Seebeck coefficient, any other material with as large Seebeck coefficient would also result in as large open circuit voltage.

A theoretical question arises whether it is possible to describe Seebeck effect from the point of view of thermionic emission at a heterojunction. We consider thermionic emission in a simple heterojunction without band bending at open circuit condition by calculation of flux Φ of carriers in both directions through the interface and over an energy barrier (Fig. 2C):

$$|\Phi_{1-2}| = |\Phi_{2-1}|, \tag{1}$$

$$\frac{n_1 \langle v_1 \rangle}{4}\sqrt{\frac{m_2}{m_1}} = \frac{n_2 \langle v_2 \rangle}{4}\sqrt{\frac{m_1}{m_2}} \cdot \exp\left(-\frac{\Delta E_c}{kT_2}\right). \tag{2}$$

Here $n_{1,2}$ are electron concentrations, $m_{1,2}$ are effective masses in each of the materials, $<v_1>$ is mean thermal velocity of cold electrons at a temperature T_1, $<v_2>$ is mean thermal velocity in the hot electron gas at a temperature $T_2 > T_1$, ΔE_C is energy barrier for electrons. The flux density $\frac{n\langle v \rangle}{4}$ is known from kinetic molecular theory of ideal gas, applicable to electrons within effective mass approximation. The exponent term describes the probability for carriers to surpass a barrier ΔE_C in approximation of Boltzmann distribution. One readily arrives at the known Richardson formula for thermionic emission by substituting the mean thermal velocity and a classical expression for the electron concentration in the nondegenerated semiconductor within the effective mass approximation [12] into equation (2)

$$<v>=\sqrt{\frac{8kT}{\pi m}}, \tag{3}$$

$$n = \frac{2(2\pi mkT)^{3/2}}{h^3}\exp\left(-\frac{E_C - E_F}{kT}\right). \tag{4}$$

Here h is Planck's constant, E_C and E_F are energy of the conduction band edge and the Fermi level. An additional correction term (square root of the effective mass ratio) is necessary in equation (2) in order to account for a change in the carrier mass after penetration through the interface, an effect not observed for molecules of the ideal gas. The form of the correction term results from consideration of (1) at equilibrium.

If $T_1 \neq T_2$, the electron Fermi level splits at the interface, whereas the split is equal to qV_{OCE}:

$$E_{F_1} = E_{F_2} + qV_{\mathrm{OCE}}. \tag{5}$$

Here V_{OCE} is part of the open circuit voltage due to hot electrons. As it follows from the band diagram in Figure 6:

$$E_{C_1} = E_{C_2} + \Delta E_C. \tag{6}$$

By substitution equations (3)–(6) into (2) for $m_1 \neq m_2$, $T_1 \neq T_2$ and resolving the equation for V_{OCE} we obtain:

$$V_{OCE} = -\frac{\Delta T}{T}\frac{E_{C_1} - E_{F_1}}{q} - \frac{2kT}{q}\left(1 + \frac{\Delta T}{T}\right)\ln\left(1 + \frac{\Delta T}{T}\right). \quad (7)$$

Here $\Delta T = T_2 - T_1$. If $\Delta T \ll T_{1,2}$, which is rather common for contemporary hot carrier solar cells, Taylor's series expansion of the logarithmic function up to the linear term results in

$$V_{OCE} = -\frac{k}{q}\left[-\frac{E_{F_1} - E_{C_1}}{kT} + 2\right]\Delta T = S\Delta T. \quad (8)$$

Equation in square brackets in (8) is a specific case of Pisarenko relation for Seebeck coefficient of the nondegenerated electron gas [13, 14]:

$$S = -\frac{k}{q}\left\{-\frac{E_{F_1} - E_{C_1}}{kT} + \left(r + \frac{5}{2}\right)\right\}. \quad (9)$$

Here r is the exponent of the energy in the expression for the carrier relaxation time from approximation of the collision term in the Boltzmann kinetic equation:

$$\tau(E) = CE^r, \quad (10)$$

and C is a constant. The value of $r = -1/2$ results from a model of free carriers of a constant scattering cross section, for which the thermal velocity is proportional to the square root of the kinetic energy. In conclusion, the open circuit voltage through thermionic emission of the hot electrons in a heterostructure is equivalent to Seebeck effect in a narrow temperature range, valid at least for the nondegenerated semiconductors.

Experimental

Prototype fabrication

Double side polished epi-ready (100) ZnTe $10 \times 10 \times 0.4$ mm³ wafers doped by phosphorus to a hole concentration of $1 - 1.2 \times 10^{17}$ cm^{-3} were purchased from JX Nippon Mining & Metals. The wafers were split in $5 \times 5 \times 0.4$ mm³ chips. Each chip substrate was etched for 20 sec in 0.4 %v bromine (Alfa Aesar, 99.8 %, CAS: 7726-95-6) solution in methanol (Carl Roth, ≥99.95 %, CAS: 67-56-1) prior to evaporation of a silver (Carl Roth, ≥99.9 %, CAS: 7440-22-4) back contact. Silver was evaporated in a vacuum deposition system B30.2 (VEB Hochvakuum, Jevatec GmbH, Jena, Germany) at P = 3×10^{-5} mbar. The top surface of ZnTe substrates was sequentially polished with 0.1 μm diamond paste and 20 nm SiO_2 slurry. Then the ZnTe chips mounted on a copper tape conductor were temporary sealed by polyimide tape with Ø 3 mm aperture. Open ZnTe surface was etched for 20 sec in the bromine-methanol solution, rinsed in the double deionized ($\sigma < 0.1$ μS) water and then placed into an electrochemical cell under an anodic potential. The aqueous electrolyte contained 0.05 M $Pb(NO_3)_2$ + 0.001 M Se + 0.5 M $Cd(NO_3)_2$ at pH = 2 corrected by HNO_3. It was deaerated with nitrogen in a three-electrode electrochemical cell prior to the deposition. The chemicals were at least 99.9% grade purchased from Carl Roth and Alfa Aesar. The potential of the working electrode was controlled by a potentiostat (VersaSTAT 4, Princeton Applied Research, Oak Ridge, TN, USA) in the three-electrode cell and measured against the saturated silver–silver chloride electrode ($Ag/AgCl/KCl_{sat}$). A Ø 3.5 mm × 50 mm glassy carbon rod (Alfa Aesar) was used as the auxiliary electrode. The electrochemical deposition was performed at a potential slightly more positive than that of bulk lead reduction. The rate of cathodic reaction of PbSe formation was limited by the Se concentration. Since the PbSe formation requires electrons on p-ZnTe surface, the deposition was performed under the illumination of a light emission diode (8.7×10^{-4} W, 460 nm). The temperature of the electrolyte was stabilized at room (24°C) temperature. Potential of the p-ZnTe substrate as the working electrode was varied in time for controlling the PbSe film composition. Analysis of the film structure, chemical composition and crystalline properties was performed using a scanning electron microscope (Ultra 55, Carl Zeiss AG, Oberkochen, Germany) with a field electron emitter, equipped with EDX and EBSD units (Bruker Corporation, Billerica, MA, USA). Acceleration voltage was 30 kV. A composition ratio of Pb:Se = 1:1 was confirmed by EDX analysis of thicker (300–600 nm) PbSe films. The top transparent electrode and the second heterojunction were produced by sputtering 100 nm of n-ZnO on top of the p-ZnTe/PbSe structure. A gauze of Ø 135 μm stainless steel wires resulting in 530×530 μm² cells was used as a hard mask for structuring of top n-ZnO layer. The ZnO(99) Al(1)wt% target with 3N5 purity was purchased from FHR Analgebau GmbH, Ottendorf-Okrilla, Germany. The magnetron sputtering of ZnO, combined with the bonding of back silver contact to the massive copper plate, was done at an argon pressure of 2×10^{-3} mbar, at an RF power of 150 W and at a substrate temperature of 200°C.

Optoelectrical measurements

The individual cells were contacted by a spring loaded pin in all electrical measurements. The I-V measurements were done using Keithley 2401 source meter controlled by ReRa Tracer software (ReRa Solutions BV, Nijmegen, Niederlands). For the illuminated I-V measurements, the

natural sunlight was focused by a 61 mm diameter glass lens with a focal length of 145 mm. The sunlight intensity was monitored by a calibrated reference solar cell type RS-00-1 (Fraunhofer ISE, Freiburg, Germany). Due to particular optical absorption in the atmosphere, related to the weather conditions, the spectral power density function continuously changes in time. Some part of this optical absorption that is due to N_2 and O_2 molecules is constant and is always present. Additional scattering may originate from eventual water droplets ("clouds"). On a sunny day, when the spectral power density is at its maximum, with the elevation of Sun of 41.8°, the "air mass" is 1.5 and the conditions are close to the "terrestrial 1 Sun" fixed in the Standard Test Conditions for solar cells. At these conditions, any calibrated solar cell will produce its rated short circuit current. If additional scattering due to moisture in the atmosphere is present, the short circuit current of the reference solar cell will be below the rating and the spectral power density function will randomly deviate from the standard test conditions. In our experiments we assured that the output of the reference solar cell was close to its rating, meaning that the spectral power density function is close to the standard one. The open circuit voltage versus temperature was measured using a digital voltmeter, whereas the temperature was controlled by a Peltier element and measured by a digital thermometer. The measurement was taken in an electrically shielded desiccator. Samples were illuminated by a 658 nm laser diode module, equipped with a focusing optics (Thorlabs, Dachau/Munich, Germany) and a silicon monitor diode. The laser module output power was calibrated according to the absolute thermal reference measurements.

Results and Discussion

We fabricated a double heterostructure according to the idea of Figure 2B on a (100) p-doped zinc telluride (ZnTe) substrate. ZnTe has zincblende structure type with a lattice constant of 0.6103 nm [15] and a band gap of 2.27 eV at 300 K [16]. A lead selenide (PbSe) film of 20 nm thickness, according to the Faraday law, was deposited by the electrochemical epitaxy [6, 17]. PbSe has the rock salt structure type, with a lattice constant of 0.6117 nm [18], and a band gap of 0.28 eV [19]. Figure 4 shows scanning electron microscopy (SEM) micrographs of the circular region where PbSe film was deposited. The region is visible at low magnification due to a mass difference of the constituting atoms in the substrate and in the film. The surface of the film remains microscopically rather smooth, so that the origin of the contrast is not related to an eventual change in the surface morphology. Pole figure, obtained by the electron backscattering diffraction (EBSD) shown in Figure 4B as the inset, confirms the epitaxial growth of the film.

The negative transparent contact was deposited by the magnetron sputtering of 100 nm ZnO doped with 1% Al_2O_3. ZnO layer having a band gap of 3.37 eV [19] was deposited through a mask, forming 0.24 mm^2 square areas (Fig. 5B). The areas in the middle part of the sample are located on top of the deposited PbSe layer, whereas ZnO was deposited directly on ZnTe at the circumference of ZnTe substrate. Both area types were illuminated by the solar radiation at various concentrations. The intensity of the solar radiation was monitored by short circuit current of a silicon reference solar cell. The measured current was 77–91% of the standard current corresponding to one Sun. The cell under investigation was contacted at the rear side by an evaporated silver layer and bonded at 200°C in vacuum/argon to a massive copper plate. During the I-V measurements, the temperature of the copper plate was in the range 49–55°C. At these test conditions, I-V characteristics shown in Figure 5C were measured.

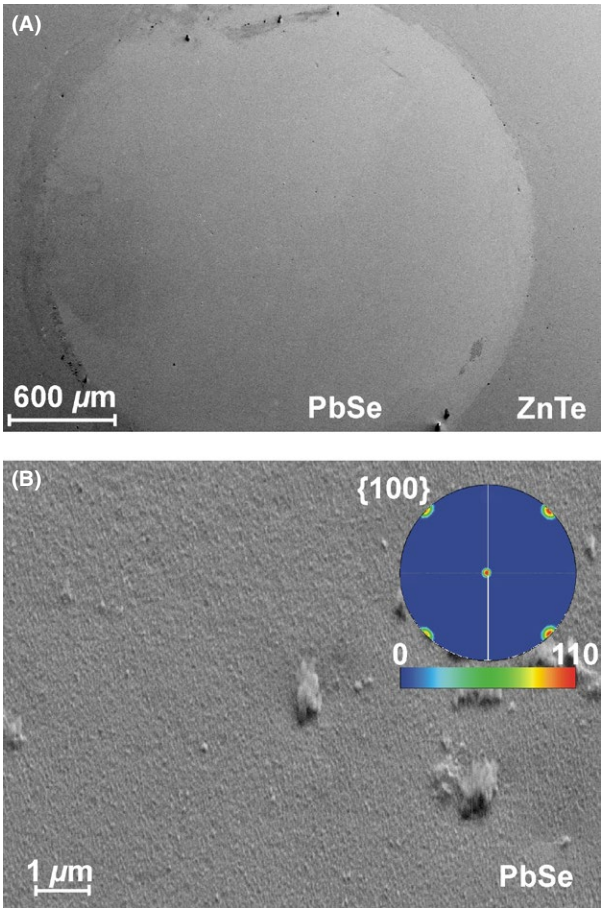

Figure 4. Scanning electron micrographs of 20 nm PbSe film on ZnTe. (A) Plan view of the PbSe thin film (circular region). (B) Tilted (70°) micrograph in the center of the covered region. Inset shows the pole figure obtained by the EBSD in the whole area of the micrograph B), confirming the epitaxial growth. The EBSD patterns were analyzed at 8153 pixels, resulting in 114 zero solutions (1.7%).

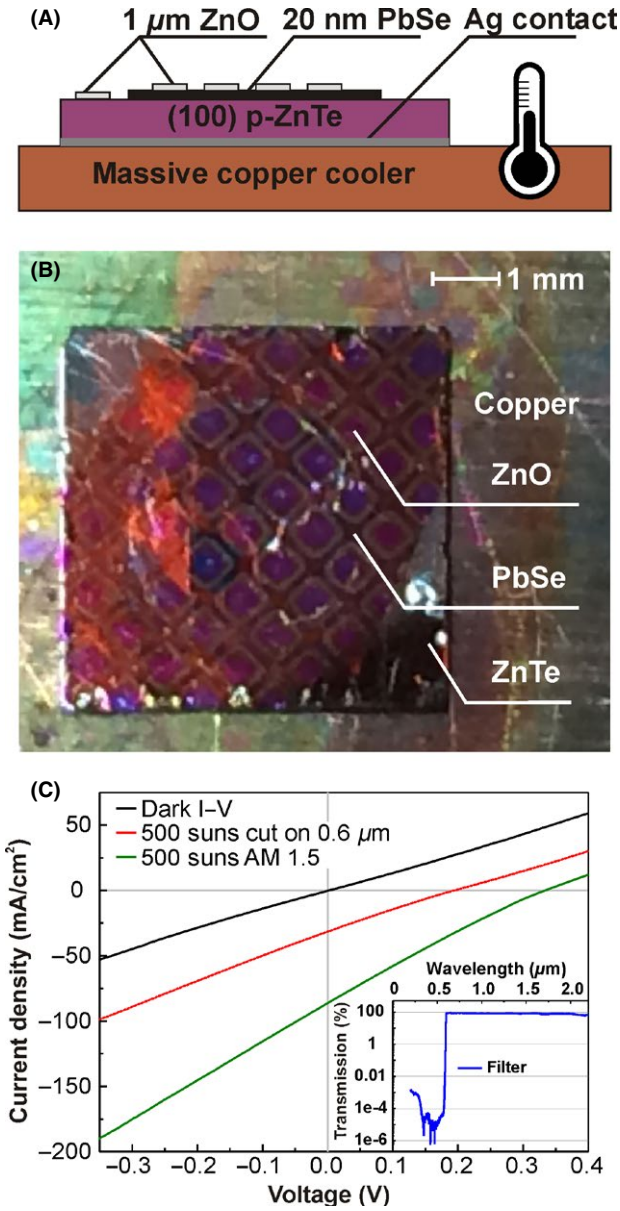

Figure 5. Hot carrier solar cell under test: (A) the layered structure of p-ZnTe/PbSe/n-ZnO double heterostructure bonded to copper cooler; (B) a plan view of the prototype: the circular region in the middle is the PbSe film; (C) the I-V characteristics of the hot carrier solar cell prototype in the dark, under concentrated (×500) and filtered concentrated (×500) sunlight; inset: the spectral characteristic of the long pass filter.

The band offsets at ZnTe/PbSe and PbSe/ZnO interfaces [19, 20] are shown in Figure 6. The band diagram implements the idea of the hot carrier solar cell in Figure 2B. Despite the small absorption in the thin PbSe film, there is a distinct improvement of the photo response in the structures with the PbSe absorber: while the structures with PbSe show open circuit voltage of 25 mV at 1 Sun and 180 mV at 15 Suns, the open circuit voltage of the ZnTe/

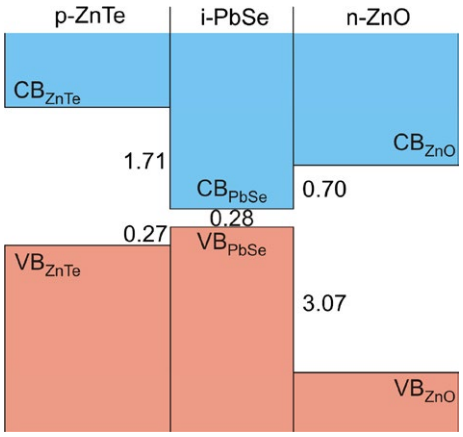

Figure 6. Band alignment in the double heterostructure ZnTe/PbSe/ZnO [19, 20]. The numbers shown near the interfaces are the band offset in electronvolts.

ZnO structure shows only 7 mV and 65 mV, respectively. Although a part of the solar spectrum is absorbed in ZnTe and results in some additional photo response, the major contribution originates from carriers in PbSe. Photocarriers originating from the ZnTe substrate may contribute to the photovoltage, if the prototype is excited in the spectral region at a wavelength below the absorption edge of ZnTe (520 nm). One of the I-V characteristics in Figure 5C was measured under concentrated solar illumination with the shortwave portion of the spectrum below 600 nm blocked by a filter. The solar cell continues to operate also at the filtered illumination conditions. We illuminated the solar cell with 1885 nm laser radiation and also measured a small photovoltage by using a lock-in amplifier. The open circuit voltage of the device under concentrated sunlight, 0.33 V, exceeds the bulk band gap of the PbSe material at room temperature, being 0.28 eV [19]. The quantum confinement in a 20-nm-wide quantum well is expected to result in a band gap evolution up to 0.318 eV [21]. This phenomenon can be explained by the diffusion of the hot carriers out of the absorber material prior to their cooling. The characteristic length L_c of hot carrier diffusion process is the hot carrier cooling length [22] with respect to the carrier cooling time τ_C, so that $L_C = \sqrt{D_C \tau_C}$, where $D_C = \mu_C kT/q$ is carrier diffusion coefficient and μ_C is carrier mobility. Assuming a temperature of 300 K, a carrier cooling time of 10 ps and a carrier mobility of μ_C = 1000 cm^2/V s, one can obtain an L_C (PbSe) = 160 nm for both electrons and holes. Hot carrier cooling length is thus significantly larger than the thickness of the PbSe absorber in the prototype (20 nm). Therefore, the hot carriers are expected to leave the absorber before cooling down. The photovoltage due to hot carriers depends on the Seebeck coefficients in ZnTe and ZnO at their specific doping levels, and on the carrier temperature in the PbSe absorber.

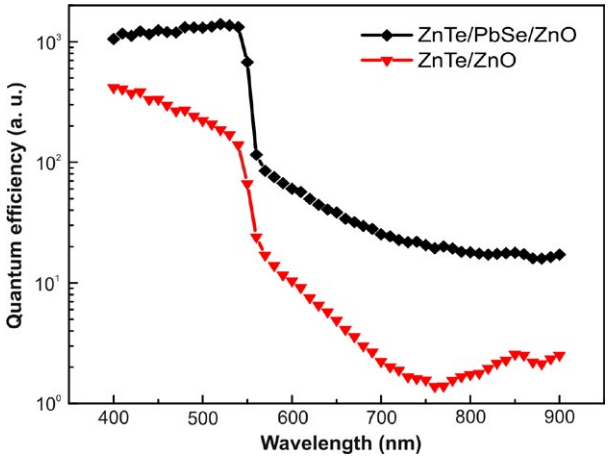

Figure 7. Quantum efficiency of the double heterostructure ZnTe/PbSe/ZnO (diamonds) and of the single heterostructure ZnTe/ZnO without the PbSe absorber layer (triangles) at low illumination intensity. The carrier collection in the 20-nm-thick absorber layer is demonstrated in the infrared region.

The upper graph in Figure 7 shows the quantum efficiency of complete double heterostructre ZnTe/PbSe/ZnO under small illumination intensity, whereas the lower graph shows the same for a reference heterostructure ZnTe/ZnO without the PbSe absorber layer. The absorption region of ZnTe is below 560 nm, resulting in additional strong photoresponse due to carrier collection in ZnTe. The lower photoresponse of ZnTe without PbSe may be related to sputtering damage of ZnTe during ZnO deposition. The structure with PbSe absorber shows at least one order of magnitude larger photoresponse in the infrared region, proving the existence and role of the absorber layer in the carrier collection, although the escape of cold carriers from the absorber is hindered by the band offsets.

The Seebeck coefficients were estimated in both ZnTe and ZnO. The ZnTe crystal of the same charge as used for the deposition was contacted by a copper foil at room temperature and by a hot metallic electrode at 550 K at its corner. A Seebeck coefficient of 430 μV/K was estimated. A ZnO film was sputtered on the soda lime glass at the identical conditions as during deposition of the heterostructures. Similarly measured Seebeck coefficient in ZnO was −67 μV/K. The difference of the Seebeck coefficients amounts to 500 μV/K. Under assumption that the open circuit voltage results only from the thermo power of the hot carriers generated in PbSe, the temperature of carriers in absorber reaches 600 °C at ×500 sunlight concentration. The lattice temperature in the double heterostructure at ×500 suns was roughly estimated from the 1D model of the transverse heat conductivity from the surface of the ZnTe wafer to the copper base plate (Fig. 5A). Only a lattice thermal conductivity coefficient of 0.18 W cm^{-1} K^{-1} [23] was considered. The temperature difference between the faces of the wafer is expected to be 13 K at ×500 suns concentration. Therefore, it can be assumed that the maximum lattice temperature at the double heterostructure does not exceed 70°C being dramatically smaller than the estimated carrier temperature.

From the points of view of both the thermionic emission and the diffusion theories of charge transport in a junction, the relation between the open circuit voltage of a solar cell and its temperature is linear with the intercept at 0 K being the activation energy of the dominant charge transport mechanism in electronvolts [24]. For example, Figure 8A shows this relation for a conventional single crystalline silicon solar cell for two different photon fluences. Both the relations are linear in a narrow temperature range close to the room temperature and both of them can be extrapolated to a common intercept at about 0 K with its value close to the band gap of silicon in electronvolts. A similar measurement with the prototype hot carrier solar cell results also in a linear function, suggesting the thermionic nature of the current flow (Fig. 8B). However, the intercepts at 0 K strongly depend on the photon fluence. The magnitude of the intercepts is close to the smaller of the measured band offsets. The photon energy in this experiment was chosen smaller than the band gap in ZnTe, so that the carrier generation took place predominantly in PbSe layer. This experimental result may be considered from the kinetic point of view by consideration of different thermionic emission situations. If the carrier temperature is the same throughout the structure, the quasi-Fermi levels for electrons are the same in PbSe and in ZnO, whereas the quasi-Fermi levels for holes are the same in PbSe and in ZnTe (Fig. 8D left). The open circuit voltage, also extrapolated to 0 K, cannot exceed the band gap of PbSe in electronvolts (we expect no population inversion in PbSe through simple optical excitation in this material). At a larger illumination intensity, the carrier temperature in PbSe may become higher than both in ZnTe and ZnO, so that the three layers are out of thermodynamic equilibrium and the electrochemical potential (quasi-Fermi levels) exhibits an offset at the interfaces (Fig. 8D right). The potential barrier height for the current of the thermionic emission flowing across the barriers at the interfaces includes additional energy of the band offsets, so that it is larger than the band gap in PbSe. Therefore, the linear function *Voc* versus temperature extrapolates to the voltages higher than the band gap in absorber in electronvolts. This is another evidence of the hot carrier filtering in the structure. On the other hand, the open circuit voltage represents a thermoelectric

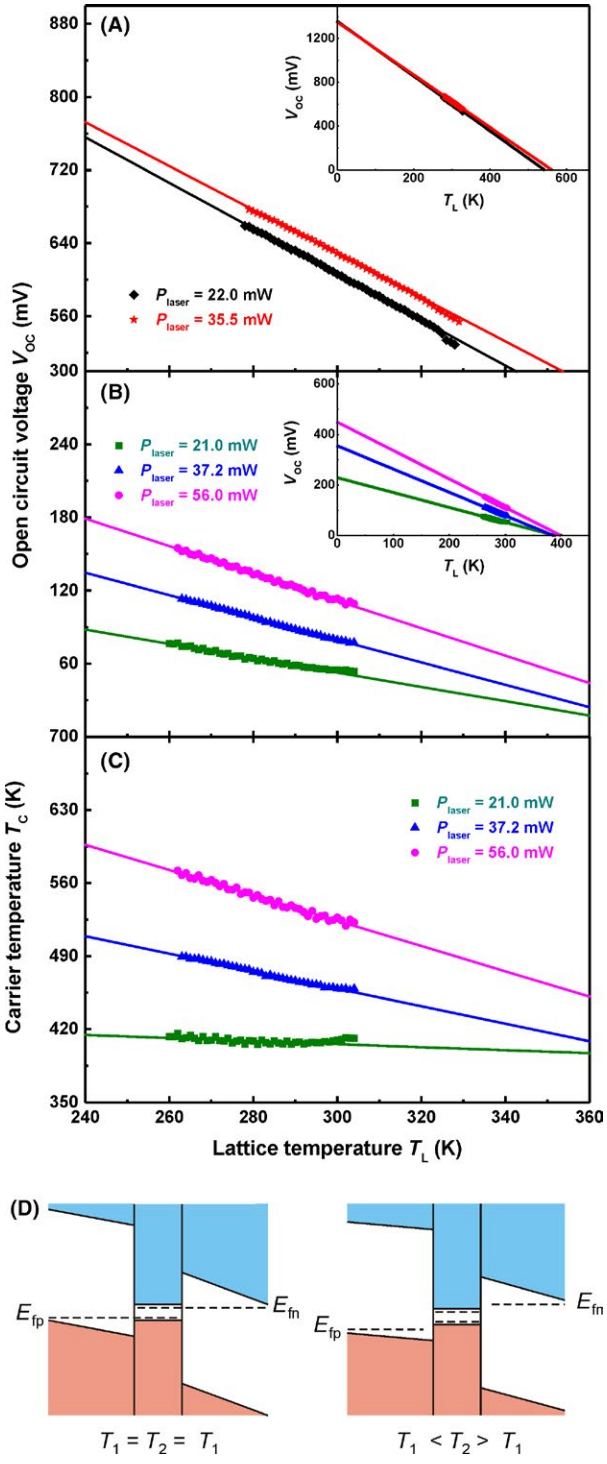

Figure 8. Open circuit voltage versus temperature due to the optical excitation at 658 nm for (A) conventional silicon solar cell; (B) prototype hot carrier solar cell; (C) carrier temperature versus the lattice temperature at various excitation power; (D) illustration of the origin of variable activation energy.

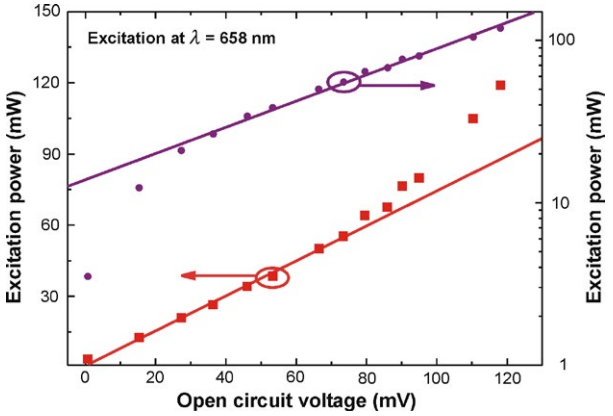

Figure 9. Suns-V_{OC} characteristics as a linear (lower) and as a semilogarithmic (upper) plots. The measurement data are the same. The optical excitation is at 658 nm, the temperature is 300 K.

voltage, showing linear dependence on the temperature difference according to the Seebeck coefficients:

$$V_{OC} = S\left(T_H - T_L\right). \tag{11}$$

The hot carrier temperature T_H can thus be calculated from the measured lattice temperature T_L, if the thermovoltage V_{OC} and the difference of the Seebeck coefficients S are known. Figure 8C shows, that the hot carrier temperature depends linearly on the lattice temperature:

$$T_H = AT_L + B. \tag{12}$$

Here, A is the slope and B is the intercept of the linear dependence of T_H on T_L, both being functions of the illumination intensity. Substitution of equation (12) into (11) shows that V_{OC} still depends linearly on the lattice temperature, but with the slope being dependent on the illumination intensity:

$$V_{OC} = S(A-1)\,T_L + SB. \tag{13}$$

This behavior is indeed observed in experiment in Figure 8B.

Close to linear I-V characteristics like that in Figure 5C are a typical feature of thermoelectric converters in general. We performed *suns*-V_{OC} measurements [25] in order to exclude the influence of the series resistance and still obtained close to linear characteristic (Fig. 9 lower plot). A narrow gap semiconductor in the middle of a p-n diode represents an interface recombination path, dominating in the carrier transport. The ideality factor in a wide-gap heterojunction of Type II, dominated by the interface recombination, is expected to be [26] close to 2. An ideality factor of 2.3 may be deduced from a

semi-logarithmic plot of the same dataset (Fig. 9 upper plot). This example illustrates two points of view on the same experiment.

Summary

In summary, we have demonstrated two equivalent approaches to describe operation and properties of hot carrier solar cells. While the common approach considers the structure as a diode where the thermionic emission takes place, an alternative approach of a thermoelectric device based on Seebeck effect is also valid. Theoretical consideration of the thermionic emission over a barrier in a heterostructure leads to a known Pisarenko relation for Seebeck coefficient. It follows from the thermoelectrical approach, that open circuit voltage of a hot carrier solar cell does not depend on interface properties of the heterostructure like band offsets, but is determined by the difference of bulk Seebeck coefficients in the energy selective contacts. A successful operation of the hot carrier solar cell prototype, based on the double heterojunction design, was demonstrated at the room temperature. The open circuit voltage of the prototype under concentrated sunlight exceeded the band gap in the bulk absorber material. The activation energy of the carrier transport is not constant, but depends on the excitation intensity. Surprisingly, the carrier temperature increases with decreasing lattice temperature at high excitation intensity. The shape of the I-V characteristics is close to linear, being common for thermoelectric devices.

Acknowledgments

We acknowledge endowed professorship of Carl Zeiss Foundation, financial support of Land Thüringen and European Commission through RFAproPV project and though Photograd network. We thank Ralf Linke (Innovent e. v. Jena, Germany) for x-ray photoelectron emission measurements for elucidation of the band diagram.

Conflict of Interest

None declared.

References

1. Ross, R. T., and A. J. Nozik. 1982. Efficiency of hot carrier solar energy converters. J. Appl. Phys. 53:3813.
2. Würfel, P. 1997. Solar energy conversion with hot electrons from impact ionization. Sol. Energy Mater. Sol. Cells 46:43.
3. Würfel, P., A. S. Brown, T. E. Humphrey, and M. A. Green. 2005. Particle conservation in the hot-carrier solar cell. Prog. Photovoltaics Res. Appl. 13:277–285.
4. Green, M. A. 2006. Third generation photovoltaics: advanced solar energy conversion. Springer-Verlag, Berlin Heidelberg, Germany.
5. Konovalov, I. 2013. Schichtenfolge zur photoelektrischen Umwandlung von Licht sowie Hot Carrier Solarzelle. German patent application DE 10 2013 105 462.5
6. Konovalov, I., V. Emelianov, and R. Linke. 2015. Hot carrier solar cell with semi infinite energy filtering. Sol. Energy 111:1–9.
7. Dimmock, J. A. R., S. Day, M. Kauer, K. Smith, and J. Heffernan. 2014. Demonstration of a hot-carrier photovoltaic cell. Prog. Photovoltaics Res. Appl. 22:151–160.
8. Dimmock, J. A. R., M. Kauer, P. N. Stavrinou, and N. J. Ekins-Daukes. 2015. A metallic hot carrier photovoltaic cell. In *SPIE Physics, Simulation, and Photonic Engineering of Photovoltaic Devices*, 9358, 935810, SPIE. https://doi.org/10.1117/12.2077573
9. Le Bris, A., and J.-F. Guillemoles. 2010. Hot carrier solar cells: achievable efficiency accounting for heat losses in the absorber and through contacts. Appl. Phys. Lett. 97:113506.
10. Mora-Sero, I., L. Bertoluzzi, V. Gonzalez-Pedro, S. Gimenez, F. Fabregat-Santiago, K. W. Kemp, E. H. Sargent, and J. Bisquert. 2013. Selective contacts drive charge extraction in quantum dot solids via asymmetry in carrier transfer kinetics. Nat. Commun. 4:2272.
11. Würfel, P. 2000. Physik der solarzellen (German Edition) Springer-Verlag, Berlin Heidelberg, Germany.
12. Sze, S. M., and K. N. Kwok. 2006. Physics of semiconductor devices, 3rd ed. John Wiley & Sons Inc, New York.
13. Bonch-Bruevich, V. L., and S. G. Kalashnikov. 1977. Semiconductor physics. Nauka, Moscow.
14. Ioffe, A. F. 1957. Semiconductor thermoelements and thermoelectric cooling. *Infosearch*. ISBN: 9780850860399
15. Hass, K. C., and D. Vanderbilt. 1987. Bond relaxation in Hg1−x Cd x Te and related alloys. J. Vac. Sci. Technol., A 5:3019.
16. Adachi, S.. 2009. Properties of semiconductor alloys: group-IV, III – V and II – VI semiconductors. John Wiley & Sons, Ltd, Chichester, UK.
17. Froment, M., L. Beaunier, H. Cachet, and A. Etcheberry. 2003. Role of cadmium on epitaxial growth of PbSe on InP single crystals. J. Electrochem. Soc. 150:C89.
18. Marinno, A. N., and K. L. Chopra. 1967. Polymorphism in some IV-VI compounds induced by high pressure and thin-film epitaxial growth. Appl. Phys. Lett. 10:282.
19. Cai, C. F., B. P. Zhang, R. F. Li, H. Z. Wu, T. N. Xu, W. H. Zhang, and J. F. Zhu. 2012. Band alignment determination of ZnO/PbSe heterostructure interfaces by

synchrotron radiation photoelectron spectroscopy. Europhys. Lett. 99:37010.
20. Konovalov, I., V. Emelianov, and R. Linke. 2016. Band alignment of type I at (100)ZnTe/PbSe interface. AIP Adv. 6:6.
21. Allan, G., and C. Delerue. 2004. Confinement effects in PbSe quantum wells and nanocrystals. Phys. Rev. B Condens. Matter. Mater. Phys. 70:1–9.
22. Kerner, B. S., and V. V. Osipov. 1976. Stratification of a heated electron-hole plasma. Sov. Phys. JETP 44:807–813.
23. Davami, K., A. Weathers, N. Kheirabi, B. Mortazavi, M. T. Pettes et al. 2013. Thermal conductivity of ZnTe nanowires. J. Appl. Phys. 114:134314.
24. Nadenau, V., U. Rau, A. Jasenek, and H. W. Schock. 2000. Electronic properties of CuGaSe2-based heterojunction solar cells. Part I. Transport analysis. J. Appl. Phys. 87:584–593.
25. Wolf, M., and H. Rauschenbach. 1963. Series resistance effects on solar cell measurements. Adv. Energy Convers. 3:455–479.
26. Grundmann, M., R. Karsthof, and H. von Wenckstern. 2014. Interface recombination current in type II heterostructure bipolar diodes. ACS Appl. Mater. Interfaces. 6:14785–14789.